

SEQUENCE ANALYSIS AND TRANSCRIPTIONAL REGULATION OF IRON ACQUISITION GENES IN TWO MARINE DIATOMS¹

Adam B. Kustka^{2,3}

Department of Geosciences, Guyot Hall, Princeton University, Princeton, New Jersey 08544, USA

Andrew E. Allen

École Normale Supérieure, Organismes Photosynthétiques et Environnement, Paris, France Department of Geosciences, Guyot Hall, Princeton University, Princeton, New Jersey 08544, USA

and François M. M. Morel

Department of Geosciences, Guyot Hall, Princeton University, Princeton, New Jersey 08544, USA

The centric diatom *Thalassiosira pseudonana* Hasle et Heimdal and the pennate diatom *Phaeodactylum tricorutum* Bohlin possess genes with translated sequences homologous to high-affinity ferric reductases present in model organisms. *Thalassiosira pseudonana* also possesses putative genes for membrane-bound ferroxidase (*TpFET3*) and two highly similar iron (Fe) permeases (*TpFTR1* and *TpFTR2*), as well as a divalent metal (M^{2+}) transporter belonging to the NRAMP superfamily (*TpNRAMP*). In baker's yeast, the ferroxidase–permease complex transports Fe(II) produced by reductases. We investigated transcript abundances of these genes as a function of Fe quota (Q_{Fe}). Ferric reductase transcripts are abundant in both species (15%–60% of actin) under low Q_{Fe} and are down-regulated by 5- to 35-fold at high Q_{Fe} , suggesting Fe(III) reduction is a common, inducible strategy for Fe acquisition in marine diatoms. Permease transcript abundance was regulated by Fe status in *T. pseudonana*, but we did not detect significant differences in expression of the copper (Cu)-containing ferroxidase. *TpNRAMP* showed the most dramatic regulation by Q_{Fe} , suggesting a role in cellular Fe transport in either cell-surface uptake or vacuolar mobilization. We could not identify ferroxidase or permease homologues in the *P. tricorutum* genome. The up-regulation of genes in *T. pseudonana* that appear to be missing altogether from *P. tricorutum* as well as the finding that *P. tricorutum* seems to have an efficient system to acquire Fe', suggest that diverse (and uncharacterized) Fe-uptake systems may be at play within diatom assemblages. Different uptake systems among diatoms may provide a mechanistic basis for niche differentiation with respect to Fe availability in the ocean.

Key index words: divalent metal transporters; ferric reductase; gene expression; iron permease; multi-copper oxidase; niche differentiation; *Pseudonitzschia*

Abbreviations: FET3, ferroxidase; FRE<n>, ferric reductase; FTR1 or FTR2, iron permease; NRAMP, natural resistance associated macrophage protein; RGE, relative gene expression; TM, transmembrane; Q_{Fe} , cellular Fe quota; $Q_{Fe90\%}$, Fe quota for 90% μ_{max} ; QRT-PCR, quantitative reverse transcription-PCR

The presence and success of diatoms fundamentally drives pelagic ecosystem structure and the efficiency of carbon export from the surface ocean (Nelson et al. 1995). Starting with the work of Martin (Martin and Fitzwater 1988, Martin et al. 1994) and others, it has become widely accepted that open-ocean assemblages of diatoms are often limited by the supply of iron (Fe; Moore et al. 2002). Despite this, surprisingly little is known of the mechanisms of Fe acquisition in diatoms. There has been mounting evidence that Fe(III) reduction is involved in this process (Anderson and Morel 1982, Maldonado and Price 2001, Shaked et al. 2005), but the identity and regulation of the enzymes responsible for Fe(II) production and subsequent uptake have not been described. The recent sequencing of the *Thalassiosira pseudonana* (Armbrust et al. 2004) and *Phaeodactylum tricorutum* genomes has provided the opportunity to probe these diatoms for the presence and expression of genes homologous to those found in other systems.

One major mechanism of high-affinity eukaryotic Fe uptake involves an initial step of Fe(III) reduction to Fe(II) at the cell surface, followed by the coupled oxidation of Fe(II) and transport of Fe(III) (Fig. 1). This reductive–oxidative mechanism of Fe acquisition has been most comprehensively studied in *Saccharomyces cerevisiae*, baker's yeast (Eide 1998,

¹Received 25 May 2006. Accepted 8 March 2007.

²Author for correspondence: e-mail kustka@marine.rutgers.edu.

³Present address: Institute of Marine and Coastal Sciences, Rutgers University, New Brunswick, New Jersey 08901, USA.

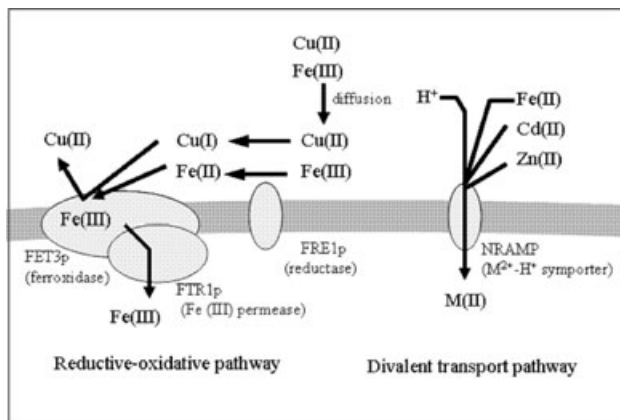


FIG. 1. An abridged schematic of Fe-uptake mechanisms in model eukaryote systems. The first step is mediated by cell-surface transmembrane NADPH-oxidoreductases (FREp), capable of reducing various Fe(III) or Cu(II) species. In *Saccharomyces*, the Fe(II) is taken up by a ferroxidase/permease complex. The Fe(II) is bound to a copper-containing ferroxidase (FET3p), subsequently oxidized by FET3p, and passed off to a ferric permease (FTR1p), which transports Fe(III) into the cell. In other systems, Fe(II) can be transported directly by divalent metal transporters, such as those in the NRAMP family. Several divalent metals, M(II), can more or less effectively compete with Fe(II) for binding and uptake.

Kosman 2003), but homologous proteins have been documented in various fungi and the green alga *Chlamydomonas reinhardtii* P. A. Dang. In yeast, the initial Fe(III) reduction is carried out by transmembrane NADPH-ferric iron oxidoreductases ("ferric reductases," designated as FRE proteins). The Fe(II) at the cell surface then binds to a copper (Cu)-containing ferroxidase (FET3p), where it is oxidized to Fe(III). Ferric Fe is then transported to an Fe(III) permease (FTR1p), which exists at the cell surface as a stable complex with FET3p (reviewed in Eide 1998, Kosman 2003). These paired reduction and oxidation/transport steps provide a degree of specificity for Fe. The only other metal known to compete with Fe uptake mediated by these proteins is Cu, as high concentrations of Cu can be reduced by reductases (Jones et al. 1987, Eide 1998) and oxidized by ferroxidases (Shi et al. 2003, Stoj and Kosman 2003).

Alternatively, Fe(II) may be transported directly into the cell without an oxidative step through a divalent metal transporter. One group of such transporters, the NRAMP superfamily, is distributed widely among prokaryotes and eukaryotes (Cellier et al. 1995). Those NRAMP proteins regulated by Fe status can also inadvertently transport other metals (Cd, Co, Mn, Zn) with varying degrees of nonspecificity (Gunshin et al. 1997, Thomine et al. 2000, Agranoff et al. 2005, Rosakis and Koster 2005). This nonspecificity seems to be characteristic of divalent metal transporters in general, including Fe(II) transporters in the zinc iron permease family (Eide et al. 1996, Eckhard et al. 2001, Cohen et al. 2004).

Here we examine the genomic data available for *T. pseudonana* and *P. tricornutum* to identify genes encoding for proteins homologous to those involved in Fe uptake in other organisms. These two diatoms were selected because complete genome sequences were available, reverse genetic manipulation methods have been or are being developed, and they are phylogenetically similar to major diatom clades in open-ocean environments. For example, strains of *P. tricornutum* have been isolated from several marine environments around the world, and phylogenetic analysis using 18S rDNA (Beszteri et al. 2001) indicates that the genus *Phaeodactylum* is closely related to the common open-ocean pennate genus *Pseudonitzschia*.

We then use quantitative reverse transcription-polymerase chain reaction (QRT-PCR) in conjunction with ^{59}Fe labeling of cells to test whether expression of putative homologues is regulated by cellular Fe status. We also tested whether other metal ions—Cd(II), Cu(II), Mn(II), and Zn(II)—could competitively inhibit Fe uptake during short-term experiments. Cu(I) is produced from Cu(II) by cell-surface reductases, and Cu(I) can be reoxidized by the ferroxidase enzyme in yeast (Shi et al. 2003, Stoj and Kosman 2003). Thus, we also examined the effects of Cu(I) on Fe uptake by using Cu(I)-specific ligands.

MATERIALS AND METHODS

Sequence analysis. Predicted gene models from the *T. pseudonana* genome (<http://shake.jgi-psf.org/Thaps3>) and *P. tricornutum* (<http://shake.jgi-psf.org/Phatr2>, access kindly provided by C. Bowler) were scanned for proteins containing NADPH-oxidoreductase domains (which include ferric reductases, FRE proteins; IPR002916), multi-copper oxidase domains (which include ferroxidases—FET3p—and laccases; IPR001117), FTR1-like Fe permease domains (IPR004923), and NRAMP domains (IPR001046). Translated sequences identified by this approach that also had transmembrane α -helix domains (TM domains) were then compared with well-characterized proteins representative of each domain family. Genomic loci and corresponding protein IDs are given in Table 1. Most of the proteins under consideration show low similarity and high divergence at the amino acid level among taxa; thus we focused our comparison on the conserved motifs involved in substrate binding or otherwise essential for enzyme activity. The relative positioning of conserved motifs and the presence of putative substrate-binding residues in diatom proteins were indicated. The TM domains were predicted using a Hidden Markov Model (Krogh et al. 2001). Figures to depict these interrelationships among proteins were made in Sigma-Plot to represent secondary structure accurately.

Three *T. pseudonana* sequences encoding for NADPH-oxidoreductases were identified, denoted as *TpFRE1-3*. *TpFRE3* (chr_1:407552-408969) is not shown in Table 1, as we did not detect any expression of this gene in preliminary experiments and did not consider it further. Two *P. tricornutum* sequences were identified and denoted as *PtFRE1* and *PtFRE2*. The amino acid sequences were compared with other transmembrane NADPH-oxidoreductases, including *Homo sapiens* respiratory burst oxidase, and two *Saccharomyces cerevisiae* and one *Arabidopsis thaliana* ferric reductases (denoted gp91^{phox}, S_tFRE1, S_tFRE2, and A_FRO2; accession numbers

TABLE 1. Genes and primers used in this study. Each gene name is as given in the text. The corresponding protein identification numbers (ID) are given underneath each gene name. Forward and reverse primer sequences and amplicon sizes are given. For some genes, two separate primer pairs were used to evaluate transcript abundance, and these are denoted as primers A and B.

Gene name	Primer sequence (5'-3') (forward/reverse)	Amplicon size	Genome locus
<i>Primers for QRT-PCR</i>			
<i>Tp</i> FRE1 (ID:11375)	gccgtacttgacaatgctga accagtgaatgcacgatga	179	chr_19c_29:203384-205714
<i>Tp</i> FRE2 (ID:3129)	atcggaagctcctgctgttt ggcctgctgtagctgacttg	145	chr_3:199111-202275
<i>Tp</i> FET3; primerA ^a (ID:5574)	gtcgtcgagcaagtctcgtt gggagcaacgtggataacat	148	chr_5:1547780-1553454
<i>Tp</i> FET3; primerB	tggatgattgagcagcaacgatc catcgtccaataaaagggtgagaa	118	
<i>Tp</i> FTR1-2; primerA (ID:268009, 20810)	gctgctgtgttttggaaattg cacctcctcctgctcgttga	95	chr_1:1226465-1227728 & chr_1:1386197-1387436
<i>Tp</i> FTR1-2; primerB	cggaggaagaggccaatcct gctccagaagcaggcgattt	122	
<i>Tp</i> NRAMP (ID:9840)	atcgccaagacgacagagtga caccgctcctagaatcccagtaatg	100	chr_14:507218-508928
<i>Tp</i> Actin (ID:25772)	actgattggagatggatgg caaagccgtaatctccttcg	162	chr_22:804575-806436
<i>Pt</i> FRE1 (ID:46928)	ggtgaaaccggaggaactc gatcattttggcgcttcatt	152	chr_11:841256-843914
<i>Pt</i> FRE2 (ID:54486)	tgtataatgcgaccagaa aagtctttgtgcgctcgatt	84	chr_8:487483-492267
<i>Pt</i> Actin (ID:29136)	tgacagagcgtggttactcg accatccatcctccaaaccac	242	chr_15:408614-412030
<i>Pt</i> TATA (ID:10199)	cggaatgcgctataaccagt accggagtcagagcacacac	175	chr_3:310168-310936
<i>Pt</i> Histone (ID:26896, 34971)	aggtcctcgcgacaatc acggaatcacgaatgacgtt	245	chr_6:764617-765260 & chr_6:779946-780351
<i>Primers for template synthesis</i>			
<i>Tp</i> full length FTR1	atgtctaattcttctaatgac ttacgctacatctgcctc	1144	chr_1:1226465-1227728
<i>Tp</i> partial length FTR2	gcatcacaacctctcacacaattt cctcggcagatacattttctcat	1184	chr_1:1386197-1387436

^aPrimer pair identical to that used in Maldonado et al. (2006).

The loci for *Thalassiosira pseudonana* and *Phaeodactylum tricoratum* genes, and the corresponding protein IDs, can be accessed at <http://shake.jgi-psf.org/Thaps3> and <http://shake.jgi-psf.org/Phatr2>, respectively.

NP_000388.2, NP_013315, NP_012702.1, and Y09581.1, respectively). We focused our comparison on the conserved motifs involved in NADPH or FAD binding, the presence and location of TM domains, and heme-coordinating residues.

A putative ferroxidase homologue in *T. pseudonana* (*Tp*FET3p) was compared with ferroxidases of *S. cerevisiae*, *Candida albicans*, *Yarrowia lipolytica*, and *C. reinhardtii* (*Sa*FET3p, *Ca*FET3p, *Yl*FET3p, *Cf*FOX1p; accession numbers CAA89768.1, CAA70509, XM_500278.1, and AAL78162.1, respectively). The position and conservation of residues involved in Cu coordination and Fe(II) binding and trafficking in *S. cerevisiae* (Taylor et al. 2005) were also compared. Only one gene model from *P. tricoratum* contained the multi-copper oxidase domain, but it did not contain any TM domains, a requirement for FET3p. In addition, TBLASTN searches ($E = 0.01$) of the *P. tricoratum* genome with *Tp*FET3 or *Cf*FOX1 did not reveal any similar genes in *P. tricoratum*.

Two putative permease homologous genes from *T. pseudonana* were identified (Table 1), *Tp*FTR1 and *Tp*FTR2. We compared the translated sequence of *Tp*FTR1 with permeases of *S. cerevisiae*, *C. albicans*, *Rhizopus oryzae*, and *C. reinhardtii* (accession numbers NP_011072.1, AAF69680, AAQ24109.1, and AAM45938.1, respectively) but omitted *Tp*FTR2p, as there is 96% nucleotide identity between the two. The presence and relative location of the Fe(III)-binding motif (encoded by the amino acid pattern REXXE, where X denotes any amino acid),

and of TM domains were compared. The presence of other motifs required for permease activity in *S. cerevisiae* ("DASE" and "EDLWE"; Severance et al. 2004) was also noted. We could not identify an FTR1 homologue in *P. tricoratum*. A subsequent TBLASTN search of the *P. tricoratum* genome with the FTR1 homologue present in *T. pseudonana* did not reveal any similar genes in *P. tricoratum* ($E = 0.1$).

A putative NRAMP-like gene from *T. pseudonana* was identified from the genome. The translated protein was compared with other NRAMP proteins: *Sa*SMF1-3, *Cs*NRAMP1, *Gm*DMT1 (*Glycine max*), and *At*NRAMP4 (accession numbers AAM54030.1, AAO39834.1, NP_201534.1, CAA64547.1, P38778, and NP_013134.1, respectively). The topologies of seven conserved motifs (Cellier et al. 1995) and the locations of TM domains were compared.

Culture conditions. Cultures of *T. pseudonana* (CCMP 1335) and *P. tricoratum* (CCMP 630) were grown in Aquil medium (Sunda et al. 2005) buffered with 100 $\mu\text{mol} \cdot \text{L}^{-1}$ EDTA using Gulf Stream water. Cells were grown at $\sim 300 \mu\text{E} \cdot \text{m}^{-2} \cdot \text{s}^{-1}$ (unless stated otherwise) under 24 h light using cool-white fluorescent bulbs. Depending on the goal of the experiment, cells were either grown under conditions of steady-state Fe availability (both species) or under conditions where Fe availability was rapidly increased (*T. pseudonana*). These conditions are referred to as "steady state" and "Fe resupply," respectively. An ^{59}Fe radiotracer approach was used to

determine cellular Fe quota. ^{59}Fe precomplexed with EDTA (1:1.05 mol:mol) was added to media and allowed to equilibrate for several hours before use. For steady-state experiments, Fe was supplied at several concentrations, from growth-limiting to excessive concentrations. This ranged from 42 to 1802 or 7–102 $\text{nmol} \cdot \text{L}^{-1}$ total Fe (*T. pseudonana* and *P. tricornutum*, respectively). These concentrations reflect the estimated Fe in our trace metal clean collected Gulf Stream water ($1.5 \text{ nmol} \cdot \text{L}^{-1}$), and an additional $0.5 \text{ nmol} \cdot \text{L}^{-1}$ from our ^{59}Fe radiotracer (specific activity = $33\text{--}84 \text{ GBq} \cdot \text{mol}^{-1}$). Fe' , the sum of all unchelated species, was calculated according to the equations of Sunda et al. (2005) at a pH of 8.3, 20°C , and $300 \mu\text{E} \cdot \text{m}^{-2} \cdot \text{s}^{-1}$. Thus, $\log K'_d$, the conditional FeEDTA dissociation constant, under our conditions was -6.40 ($\text{Fe}' = 0.004 \text{ Fe}_T$). A maximum of $\sim 750 \text{ pmol} \cdot \text{L}^{-1}$ Fe' was assumed because of iron hydroxide precipitation, but for simplicity, we report the results as Fe' even at concentrations exceeding this maximum. Steady-state uptake rates for several coastal diatoms often continue to increase with increasing Fe_T , within the region of iron hydroxide precipitation (Sunda and Huntsman 1995).

Cells were acclimated to a given Fe concentration in media without radioisotopes and were subsequently transferred to media with ^{59}Fe radiolabel. Cells were deemed to be in steady-state conditions with respect to both growth rate and isotopic labeling when the growth rate differed by $<10\%$ upon successive transfers and at least 15 generations were grown in radiolabeled media. Cell density was determined using a Coulter counter (Beckman-Coulter, Fullerton, CA, USA), and growth rates were computed from a linear regression of \ln (cell density) versus time. The error of the growth rate over the ~ 8 generations in a given culture vessel was calculated as the standard error of the slope.

During the steady-state experiments, cells were harvested for Fe quota and RNA in early to mid-exponential phase ($\sim 3 \times 10^5$ to 5×10^5 cells $\cdot \text{mL}^{-1}$). Intracellular Fe was measured radiometrically from the fraction of ^{59}Fe assimilated by cells. Cells were rinsed with the Ti-citrate-EDTA wash of Hudson and Morel (1989). Duplicate measurements were made for all quota determinations. Steady-state uptake rates, V_{ss} , were calculated as the product of steady-state growth and Q_{Fe} . For each biological replicate, a log-log plot of the computed steady-state uptake rate versus Fe' for each species fit a linear equation at low Fe' . To compare the ability of each species to take up Fe at low Fe' , we interpolated values of Fe' necessary to achieve steady-state uptake rates of $40 \text{ amol} \cdot \text{cell}^{-1} \cdot \text{d}^{-1}$.

The effect of rapid Fe resupply was determined in two independent experiments with severely Fe-limited *T. pseudonana*, grown at $170 \text{ pmol} \cdot \text{L}^{-1}$ Fe' in a 4 L polycarbonate bottle. In the first experiment, Fe was added in freshly prepared culture medium as an FeEDTA complex at a concentration of $7.2 \text{ nmol} \cdot \text{L}^{-1}$ Fe' , with a $170 \text{ GBq} \cdot \text{mol}^{-1}$ quantity of ^{59}Fe . As this concentration of Fe is supersaturating with respect to oxyhydroxide precipitation, this culture medium was prepared fresh to minimize precipitation before dilution into the culture vessel containing cells. Upon addition, the final concentration of Fe in the culture was $2.44 \text{ nmol} \cdot \text{L}^{-1}$ Fe' . In the second experiment, Fe was added at a concentration of $12.2 \text{ nmol} \cdot \text{L}^{-1}$ Fe' , resulting in a final concentration of $4.12 \text{ nmol} \cdot \text{L}^{-1}$ Fe' . Radiolabeled cells were collected (as in the steady-state experiments above), and cellular Fe was calculated at each time point by considering the uptake of ^{59}Fe -labeled Fe and the estimated cellular Fe before ^{59}Fe addition (derived from data presented in Fig. 8b at $170 \text{ pmol} \cdot \text{L}^{-1}$ Fe').

RNA extraction and QRT-PCR. Cells were harvested on 47 mm polycarbonate filters ($3 \mu\text{m}$) and frozen on liquid nitrogen until RNA extraction. Cell lysis and crude RNA separation were performed using the Trizol reagent (Invitrogen, Carlsbad, CA, USA). The resultant aqueous phase was

diluted 1:1 with 64% EtOH and subsequently purified using Ambion's RNAqueous kit (Ambion, Austin, TX, USA) according to the manufacturer's directions. We determined that 97%–99% of the ^{59}Fe was recovered in the flow through after loading the Ambion spin column. The remaining 1%–3% ^{59}Fe was removed from the column by the initial column-washing step in the Ambion kit (Ambion wash solution #1). Therefore, precautions taken for handling ^{59}Fe could be relaxed after this initial washing. The RNA elution was treated with DNase at 37°C for 30 min. The RNA concentration was determined using the fluorescent RNA probe RiboGreen (Molecular Probes, Invitrogen), and all RNA preparations were diluted to $125 \text{ ng} \cdot \mu\text{L}^{-1}$ with Elution Solution (to ensure equal concentrations for first-strand cDNA synthesis). The RNA elutions were treated with Ambion RNAqueous DNase for 30 min at 37°C . First-strand cDNA synthesis was performed with Invitrogen's Superscript III kit, using $1 \mu\text{g}$ RNA per $20 \mu\text{L}$ reaction and an oligo d(T)₂₀ primer. No reverse transcription (RT) and no template controls were carried out during each cDNA synthesis, and repeated treatments with DNase were sometimes necessary. Quantitative PCR was performed on a Stratagene Mx3000P "real-time" PCR machine (Stratagene, Cedar Creek, TX, USA) using Stratagene Brilliant SYBR Green kit according to the manufacturer's directions. For *P. tricornutum*, PCR cycling conditions consisted of 94°C for 8 min (denaturation) followed by 40 cycles of 94°C , 20 s; 53°C , 30 s; 72°C , 30 s; and melt-curve analysis starting at 53°C (30 s) with 0.5°C steps for 70 cycles. For *T. pseudonana* transcripts, the conditions were identical except that the annealing temperature was 54°C . Primer concentrations were set at $0.15 \mu\text{mol} \cdot \text{L}^{-1}$, and 5 ng transcribed RNA was used for each $40 \mu\text{L}$ reaction ($125 \mu\text{g} \cdot \text{L}^{-1}$). Copy numbers of genes of interest (GOI), relative to that of housekeepers (HK), were estimated as $2^{-(C_{\text{CHK}} - C_{\text{GOI}})}$ [shorthand as $2^{(-\Delta C_t)}$] according to Pfaffl (2001). This quantity was determined from replicate analyses for each observation, within each replicate experiment. Melt-curve analyses for each primer indicated single peaks with melting temperatures consistent with the absence of primer-dimers. This finding was confirmed by gel electrophoresis on one occasion. Standard templates were generated by gel purification of PCR products using gene-specific primers and quantified using Pico-Green fluorescent dye (Molecular Probes). Real-time PCR efficiency was calculated by plotting C_t versus \log (template copy number) from analysis of a four-point serial dilution spanning a range of 256-fold template concentration. The slope was used to calculate efficiency, $E = 10^{(-1/\text{slope})}$. The average efficiency for all genes considered was 1.97 ± 0.10 (SD). Primers used in this study are given in Table 1. For most genes, one set of reverse and forward primers was used. However, there are two homologues of *SrFTR1* in *T. pseudonana* that share 96% nucleotide identity (designated as *TpFTR1* and *TpFTR2*). We attempted to design a primer pair exclusive to *TpFTR1*, with a reverse primer (targeted toward *TpFTR1*) specifically mismatched at its 3' end with respect to the 5'-binding site of the *TpFTR2* amplicon. However, we found that this primer pair amplified both *TpFTR1* and *TpFTR2* with near equal efficiency under our conditions. Thus, we report relative gene expression (RGE) of *TpFTR1-2* to indicate a combined transcript abundance for both genes. Also, in one Fe-resupply experiment, we used two separate primer pairs to target *TpFET3* transcripts.

For experiments with *T. pseudonana*, the expression of actin was constitutive under all Fe_T concentrations tested; thus actin served as an appropriate HK gene. This was determined by a residual plot of cycle threshold (C_t) versus Fe concentration (data not shown), in which the variability of the residual C_t was small and random. Our analysis of actin C_t residue versus treatment in *P. tricornutum* seems to indicate a positive correlation between Fe_T and C_t residue, contrary to our experience

with *T. pseudonana*. Using a single HK gene whose expression appears to correlate with treatment can produce misleading results. In the case of *P. tricornutum*, we normalized the results according to three separate HK genes encoding for actin, TATA box-binding protein, and histone (see Bustin 2002). These proteins are physiologically distinct and have diverse, yet constitutive roles in the cell. We graphically report the RGE data using actin as the HK gene—for clarity of presentation—and provide the statistical analyses (described below) for gene expression data normalized to each of the three HKs.

Statistical analysis and replication. All growth and cell quota measurements were repeated for each species across a range of Fe. The RNA was extracted, and gene expression was analyzed for both steady-state experiments with *P. tricornutum*. The RNA was only available for one of the two *T. pseudonana* steady-state experiments. Rather than conducting a third steady-state ^{59}Fe -labeling experiment with *T. pseudonana* (which showed reasonable replication of growth versus Q_{Fe} between the two experiments), we directed our QRT-PCR efforts to focus on replicated experiments with transient changes in Fe supply. In the steady-state experiments, the effect of Q_{Fe} on RGE was tested by evaluating the slope of a log-log regression of RGE on Q_{Fe} within the range of Fe limitation (where $Q_{\text{Fe}} \leq Q_{\text{Fe}90\%}$, where $Q_{\text{Fe}90\%}$ is the Q_{Fe} at which $\mu \sim 90\% \mu_{\text{max}}$). As this slope is amenable to parametric statistical analyses (invoking the central limits theorem; Sokal and Rohlf 1995), we used the standard regression analysis tool available in Microsoft Excel (Microsoft Corp., Redmond, WA, USA) and report the slope, error about that slope, y-intercept, and one-tailed *P*-value for the slope. A negative slope significantly different from zero ($P < 0.05$) indicates an effect of Q_{Fe} on RGE.

In the time-course experiments, a paired comparison of each of four RGE values obtained at $t = 0$ was made with each of four combined mean RGE values for $t = 3, 6,$ and 12 h. This tests the null hypothesis that RGE at $t = 0$ is not significantly different from the RGE values obtained at 3–12 h after Fe addition. A regression analysis was deemed inappropriate a posteriori because there were less than three observations where $Q_{\text{Fe}} \leq Q_{\text{Fe}90\%}$ in each experiment.

Inhibitors of Fe uptake. Short-term uptake experiments using radiolabeled Fe (^{59}Fe) and other metals as competitive inhibitors of Fe uptake were conducted with cultures of each diatom species grown under Fe-limiting conditions. Experiments with Cu, Mn, Cd, or Zn were conducted in chelexed synthetic ocean water (SOW), amended with chelexed macronutrients (50, 5, 50 $\mu\text{mol} \cdot \text{L}^{-1}$ N, P, Si) and 0.5 $\text{nmol} \cdot \text{L}^{-1}$ ^{59}Fe (added as FeCl_3 ; conditions similar to those of Hudson and Morel 1990). Cells were gently filtered with a 3 μm polycarbonate filter, rinsed with chelexed SOW, and resuspended into experimental media. Each uptake rate was determined from four time points collected over 2–2.5 h. Experiments were conducted in the dark at room temperature (23°C). Metal stocks were made from A.C.S. grade CdCl_2 , MnCl_2 , or ultrapure grade Cu(s) and Zn(s). Cu(s) and Zn(s) were dissolved with quartz distilled HNO_3 and Milli-Q (Millipore, Billerica, MA, USA). In uptake assays involving Cu(II), additional treatments included the addition of the Cu(I)-binding ligand BCDS (bathocuproine disulfonic acid; disodium 2,9-dimethyl-4,7-diphenyl-1,10-phenanthroline disulfonic acid; Sigma, St. Louis, MO, USA) in the presence and absence of Cu(II). In these cases, we use high concentrations of Cu as an inhibitor of Fe uptake, and this should not be confused with others' efforts to investigate Cu limitation (Peers et al. 2005). For metals that showed an inhibitory effect on Fe uptake, $^{14}\text{C-HCO}_3^-$ uptake experiments were conducted under similar conditions (with the exception of lighting; data not shown) to verify that the observed effects were not caused by gross physiological impairment.

RESULTS

Sequence analysis. Putative ferric reductases from *T. pseudonana* (*Tp*FRE1-3) and from *P. tricornutum* (*Pt*FRE1-2) were identified and compared with NADPH-oxidoreductases from other organisms (Fig. 2). *Tp*FRE2 and *Tp*FRE3 in many ways resemble the yeast *Sc*FRE1 and *Sc*FRE2. The location (relative to the carboxyl terminus) and relative spacing of the NADPH- and FAD-binding motifs are nearly identical among these proteins. In addition, there are almost equal numbers of residues situated between the NADPH-adenine binding motif (squares in Fig. 2) and the nearest predicted TM domain of *Sc*FRE1, *Sc*FRE2, *Tp*FRE2, and *Tp*FRE3. For each of these four proteins, histidine residues capable of coordinating a pair of hemes are situated within or at the periphery of the predicted TM domains. In *Sc*FRE1, this pair of hemes is responsible for transferring an electron from FAD through the membrane to Fe(III) substrates (Finegold et al. 1996). All these similarities among *Sc*FRE1p, *Sc*FRE2p, *Tp*FRE1, and *Tp*FRE2 suggest similar ter-

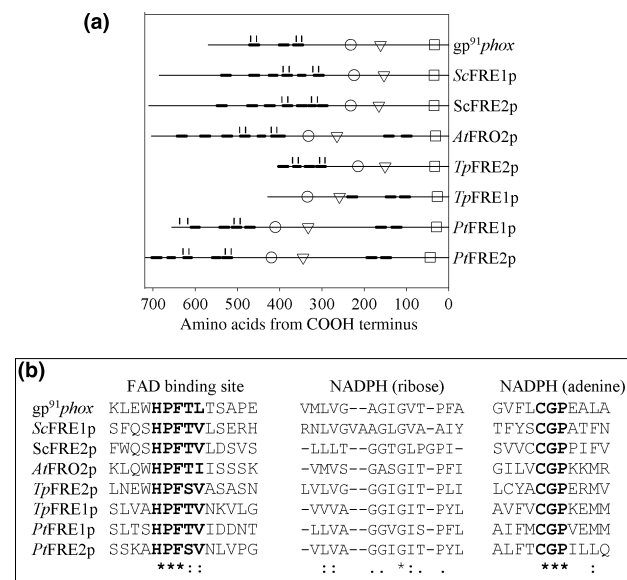


FIG. 2. Conservation of required motifs and secondary structure of transmembrane oxidoreductases. (a) Functionally conserved motifs of *gp91^{phox}* (*Homo sapiens*), *Sc*FRE1-2p, *At*FRO2p, and predicted proteins from *Thalassiosira pseudonana* and *Phaeodactylum tricornutum* gene models (*Tp*FRE1-2p, *Pt*FRE1-2p). Amino acid sequences are aligned with respect to the carboxyl terminus. FAD-isoalloxazine (circles), NADPH-ribose (inverted triangles), and NADPH-adenine (squares) binding motifs are shown. Transmembrane (TM) domains are indicated by the bubbled regions, and the histidine residues putatively involved in bis-heme coordination are depicted by vertical hatches (Shatwell et al. 1996). (b) Amino acid sequences of the conserved motifs depicted in (a), indicated in bold, and adjacent amino acids (the NADPH-ribose binding site is conserved in terms of glycine richness rather than amino acid sequence). The motifs were aligned using ClustalW; asterisks, colons, and periods represent identical, strongly similar, and weakly similar residues, respectively.

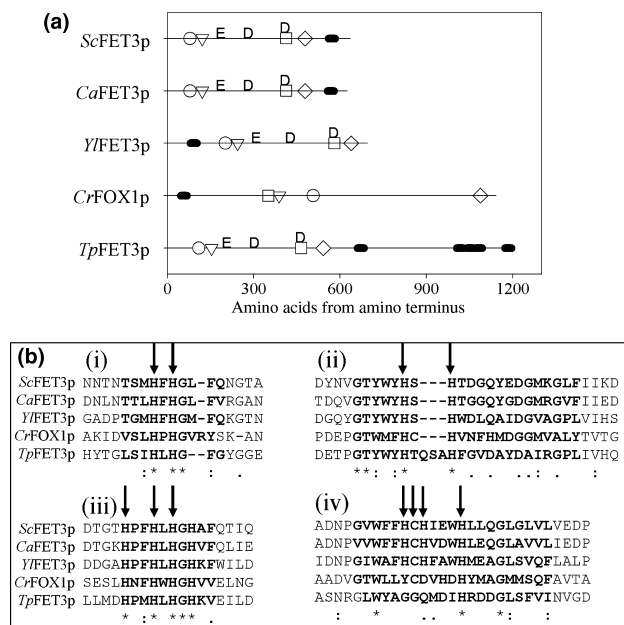


Fig. 3. Conservation of required motifs and secondary structure of copper-containing ferroxidases. (a) Relative position of copper-binding motifs and transmembrane (TM) domains for fungal (*Saccharomyces cerevisiae*, *Candida albicans*, *Yarrowia lipolytica*) ferroxidases, the *Chlamydomonas reinhardtii* ferroxidase CrFOX1, and the *Thalassiosira pseudonana* ferroxidase homologue. Binding motifs for type I and type III Cu atoms (circles); type III Cu (inverted triangles); type I, II, and III Cu atoms (squares); and type I and II Cu atoms (diamonds) were determined from alignment with demonstrated motifs present in *S. cerevisiae* (Taylor et al. 2005). Residues necessary for Fe(II) binding and trafficking (E185, D283, D409) in *S. cerevisiae* (Taylor et al. 2005) and similarly positioned residues in other proteins are indicated along each sequence. The TM domains are indicated by the bubbled regions (note that three closely spaced TM domains are present for *TpFET3p* from amino acids 1005–1093 but cannot be resolved in this figure). (b) Amino acid sequences of the conserved motifs depicted in (a) and adjacent amino acids. Roman numerals (i) through (iv) correspond to regions shown as circles, inverted triangles, squares, and diamonds in (a). Specific histidine or cysteine residues involved in Cu coordination by *ScFET3p* are denoted by arrows. Motifs were aligned with ClustalW; asterisks, colons, and periods represent identical, strongly similar, and weakly similar residues, respectively.

tiary structures for these proteins in yeast and *T. pseudonana*, and the correct orientation of motifs involved in transmembrane electron transport.

A comparison of *PtFRE2* and *AfFRO2* amino acid sequences also reveals striking similarities in the spatial arrangement of conserved motifs. Each has a pair of TM domains between the NADPH-adenine and ribose binding sites (inverted squares and triangles in Fig. 2). In this regard, the *PtFRE2* more closely resembles reductases in *A. thaliana* than *S. cerevisiae*. Nonetheless, the spacing of these TM-spanning regions positions these binding sites on the same side of the plasma membrane. In *PtFRE2* and *AfFRO2*, the histidine residues are also situated within or at the periphery of the predicted TM domains.

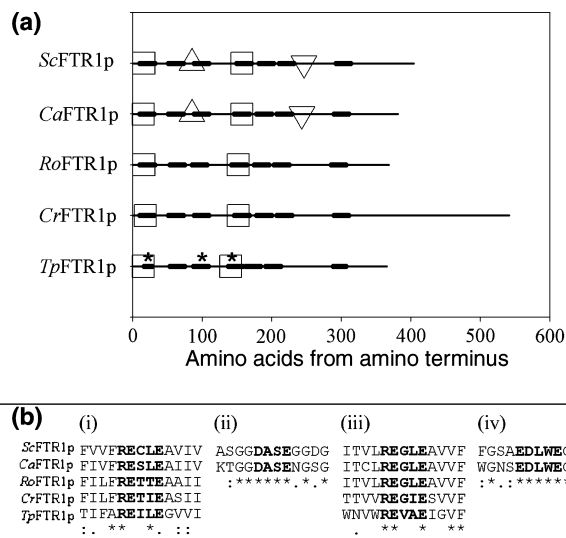


Fig. 4. Conservation of required motifs, secondary structure, and transmembrane (TM) domains of Fe permeases. (a) Fe permeases of *Saccharomyces cerevisiae*, *Candida albicans*, *Rhizopus oryzae* (all fungi), *Chlamydomonas reinhardtii*, and *Thalassiosira pseudonana* are aligned with respect to the amino terminus. Metal-binding motifs (REXXE) are indicated by squares, the motifs “EDLWE” and “DASE” (required for permease activity in *S. cerevisiae*; Severance et al. 2004) are shown as triangles and inverted triangles, and TM domains are indicated by the bubbled regions. Asterisks indicate regions of predicted hydrophobic character that were not identified as TM regions by the Hidden Markov Model (see Discussion). (b) Amino acid sequences of the conserved motifs depicted in (a), indicated in bold, and adjacent amino acids. Roman numerals (i) and (iii) correspond to regions shown as squares, while (ii) and (iv) correspond to triangles and inverted triangles in Figure 4a. Motifs were aligned with ClustalW; asterisks, colons, and periods represent identical, strongly similar, and weakly similar residues, respectively.

Two of the putative reductases identified (*TpFRE1* and *PtFRE1*) have some distinguishing characteristics. *TpFRE1* is a TM-spanning protein with the required motifs for NADPH and FAD binding, but it seems to lack (within the predicted TM domains) the histidine residues required for heme coordination in *ScFRE1p* and gp91phox (Finegold et al. 1996). In addition, if the TM domain predictions are correct, the presence of three TM domains between the adenine and ribose binding sites would suggest that these sites are situated on opposite sides of the membrane. Also, the *PtFRE1* protein has similar secondary structure to both *PtFRE2* and *AfFRO2*. However, one histidine residue is predicted to fall slightly outside of the predicted TM domain in *PtFRE1*.

The overall presence and location of required motifs for ferric reductases indicate that these proteins are suitable candidate ferric reductases. We were concerned about the missing or misplaced histidine residues of *TpFRE1* and *PtFRE1* (respectively). Despite this concern, *TpFRE1* and *PtFRE1* transcripts were relatively abundant (~ 0.15 to 0.6 relative to actin; below) and regulated by Q_{Fe} .

Histidine may be the most common heme-coordinating residue in characterized proteins and must be particularly suitable for this function. However, other amino acids [glutamic acid (E) or glutamine (Q)] have been shown to coordinate heme within individual proteins that belong to families where histidine is otherwise the “standard” heme-coordinating residue (Ikeda-Saito et al. 1992, Tanaka et al. 1997).

Members of the multi-copper oxidase family contain four Cu atoms that facilitate the oxidation of a wide variety of inorganic or organic substrates. The relative spacing of the Cu-coordinating motifs (Fig. 3a) in *T. pseudonana* is nearly identical to those in ferroxidases in *S. cerevisiae*, *C. albicans*, and *Y. lipolytica*. In addition, the residues responsible for Fe(II) binding and trafficking in ScFET3p (E185, D283, D409) may be present in the *T. pseudonana* homologue (Fig. 3a), based on their proximity to the expected active sites. Ferroxidases characterized in *S. cerevisiae* and other fungi are anchored in the cell-surface membrane by a single TM domain. T ρ FET3p has a TM domain in the same relative location as those in *S. cerevisiae* and *C. albicans*, and an additional four TM domains in the 3' region. However, there is one notable difference between the *T. pseudonana* homologue and fungal FET3 proteins. While the four motifs are similar in location and sequence among these species, three of the 11 amino residues involved in coordinating Cu in ScFET3 are absent from T ρ FET3p [the first three required residues of the fourth motif (Fig. 3b) corresponding to H483,

C484, and H485 of ScFET3p; Taylor et al. 2005]. Two of these residues are also absent from CrFOX1, which is transcriptionally up-regulated under Fe limitation (La Fontaine et al. 2002). Interestingly, the topology of the Cu-binding motifs in CrFOX1p differed from all other ferroxidases under consideration [given the dissimilar arrangement of Cu-binding motifs in CrFOX1p and ScFET3p, we did not attempt to infer the presence and locations of residues responsible for Fe(II) binding and trafficking in CrFOX1p]. Short-term Cu-resupply experiments strongly suggest the Cu-binding sites of cell-surface ferroxidases have direct access to the external milieu; from this milieu, Cu can spontaneously insert into apo-ferroxidase and restore Fe-uptake activity (Herbik et al. 2002, Peers et al. 2005, Maldonado et al. 2006). Therefore, it is possible that slight differences in binding sites may simply reflect the different chemical environments of yeast and algae.

The amino acid sequence of T ρ FTR1p was compared with other permeases (Fang and Wang 2002, Fu et al. 2004, Severance et al. 2004). The Fe(III)-binding motifs (REXXE) are present in *T. pseudonana* and other model organisms (Fig. 4). For model organisms, these motifs are situated within predicted TM domains. But for *T. pseudonana*, these motifs occur within regions of strong hydrophobic tendency that do not cross the statistical threshold of the HMM to be designated as TM domains. This finding may simply reflect the imperfections of in silico predictive models, or it may reflect true conformational differences between the diatom and

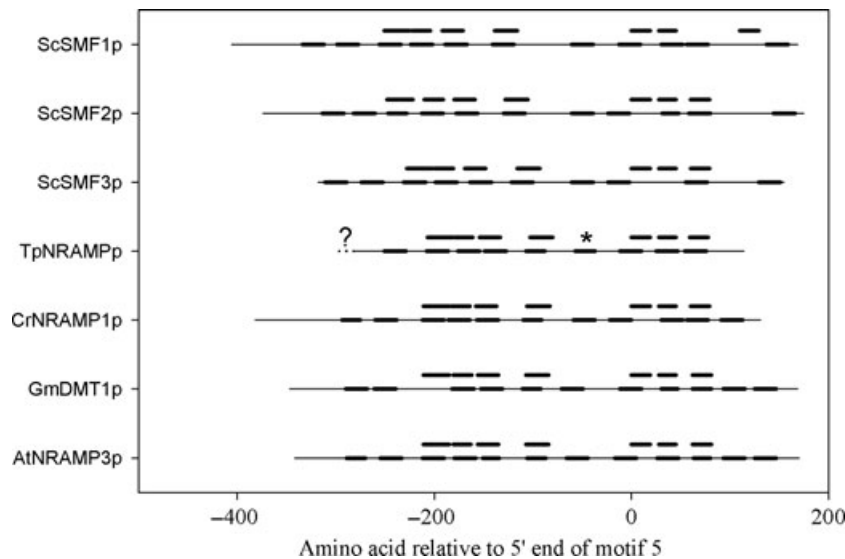


FIG. 5. Conservation of motifs in *Thalassiosira pseudonana* NRAMPp and other divalent metal transporters in the NRAMP superfamily. NRAMP sequences from yeast (ScSMF1-3), *T. pseudonana*, *Chlamydomonas reinhardtii*, *Glycine max*, and *Arabidopsis thaliana* are aligned at the amino termini of motif 5 (the putative transport motif identified by Cellier et al. 1995). The TM domains are indicated by the bubbled regions along each sequence, while bars above each sequence span the location of the seven conserved motifs. Asterisks represent identical residues. The question mark at the 5' terminus of T ρ NRAMPp and the 20-amino-acid-length dotted line indicate that the gene models for this protein have not identified a start codon.

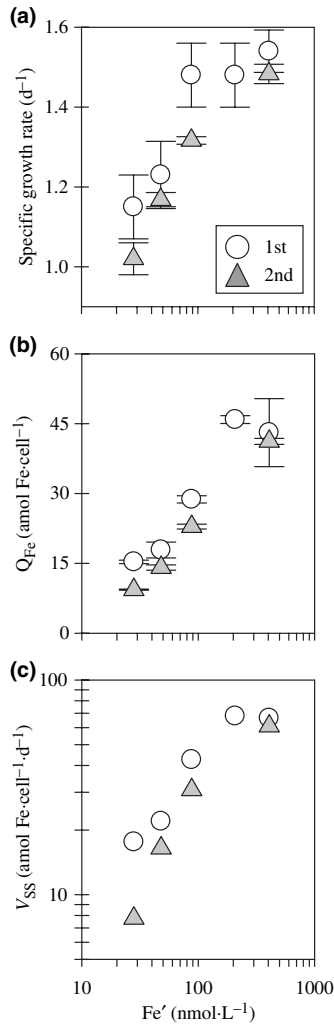


FIG. 6. Steady-state growth rates, cellular Fe quotas, and uptake rates as a function of total Fe' in *Phaeodactylum tricornutum*. For all panels, hollow circles and shaded triangles represent the first and second experiments, which are independent biological replicates. (a) Specific growth rates as a function of Fe' in culture media, ranging from 28 to 410 $\mu\text{mol} \cdot \text{L}^{-1}$. Vertical error bars represent the standard error of the slope of $\ln(\text{cell} \cdot \text{mL}^{-1})$ versus time for each culture. (b) Cellular Fe quota (Q_{Fe}) determined at varying Fe' . Vertical error bars indicate the standard deviation of cellular Fe quota based on duplicate measurements. (c) Steady-state Fe-uptake rate (the product of cellular quota and steady-state growth rate) for *P. tricornutum* versus Fe' .

fungus proteins. The Fe(III)-binding motifs may be situated on α helices with one face exposed to the aqueous phase, raising the possibility that the interactions between FTR1p and FET3p, and FTR1p and Fe(III) may very well differ between diatoms and yeast. The *T. pseudonana* FTR1p is also missing the DASE and EDLWE motifs, thought to be required for *S. cerevisiae* (Severance et al. 2004; Fig. 4). However, these motifs are also missing from other fungal permeases that have been shown, through heterologous expression, to be active (Fang and Wang 2002, Fu et al. 2004).

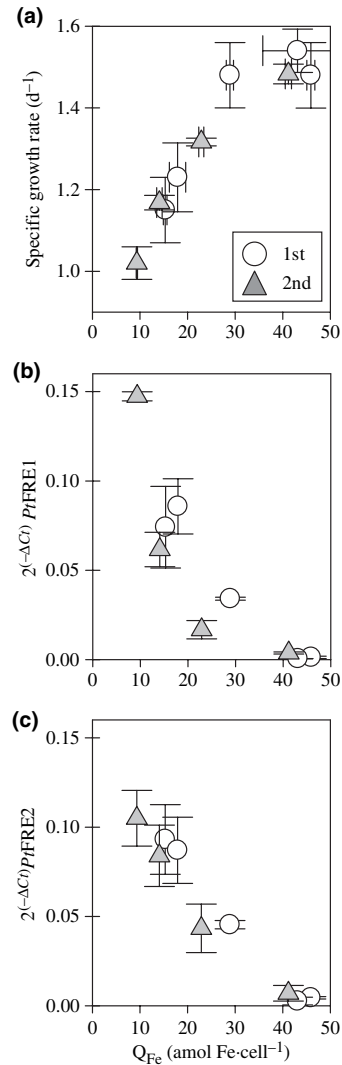


FIG. 7. Growth and relative gene expression (RGE) in *Phaeodactylum tricornutum* as a function of cellular Fe quota (Q_{Fe}). Hollow circles and shaded triangles represent the first and second experiments, which are independent biological replicates. (a) Specific growth rate versus Q_{Fe} . (b) RGE of *PtfRE1* versus Q_{Fe} . (c) RGE of *PtfRE2* versus Q_{Fe} . Vertical and horizontal error bars in panel (a) are as in Figure 6, a and b, respectively. Vertical error bars in panels (b) and (c) represent the standard deviations of duplicate RGE determinations (separate QRT-PCR runs) for each treatment.

The putative NRAMP present in *T. pseudonana* appears to have the seven conserved motifs characteristic of members of this superfamily (Fig. 5; Cellier et al. 1995). For most known NRAMPs, the transport motif (the fifth from the amino terminus) is situated between TM domains 8 and 9 but is located between TM domains 7 and 8 for *Glycine max*. It is not clear between which TM domains the transport motif is situated for the diatom protein, because the current gene model for this protein has not identified a start codon. This protein may have an additional TM domain near the 5' terminus. Our

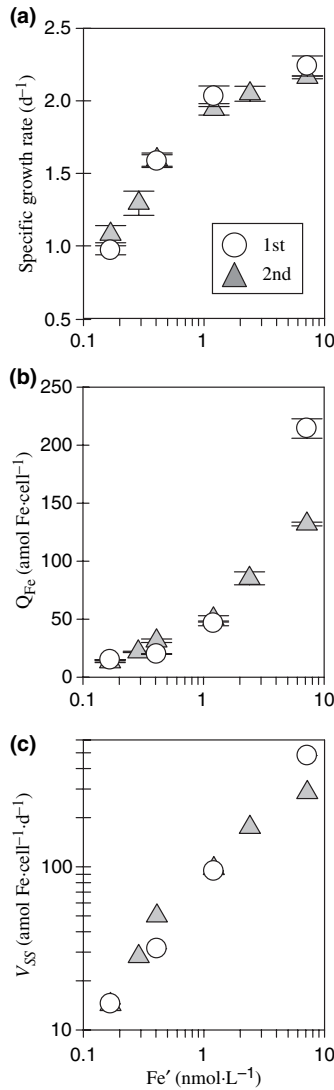


FIG. 8. Steady-state growth rates and cellular Fe quotas (Q_{Fe}) as a function of total Fe' in *Thalassiosira pseudonana*. Hollow circles and shaded triangles represent the first and second experiments, which are independent biological replicates. (a) Specific growth rates as a function of Fe' in culture media, ranging from 170 to 7200 $\mu\text{mol} \cdot \text{L}^{-1}$. Vertical error bars represent the standard error of the slope of $\ln(\text{cell} \cdot \text{mL}^{-1})$ versus time for each culture. (b) Q_{Fe} determined at varying Fe' . Vertical error bars indicate the standard deviation of cellular Q_{Fe} based on duplicate measurements. (c) Steady-state Fe-uptake rate (the product of cellular quota and steady-state growth rate) for *T. pseudonana* versus Fe' .

recent Western blotting efforts (unpublished results) reveal a single band corresponding to a ~ 57 kDa protein, similar to the sizes given for other NRAMP proteins and larger than the 43 kDa predicted by the gene model. In addition, one region where a TM domain might be expected was predicted to have hydrophobic character, similar to the situation for the permease (above). Nonetheless, the overall sequence similarity and spatial conservation suggest that this protein is likely to be an NRAMP protein.

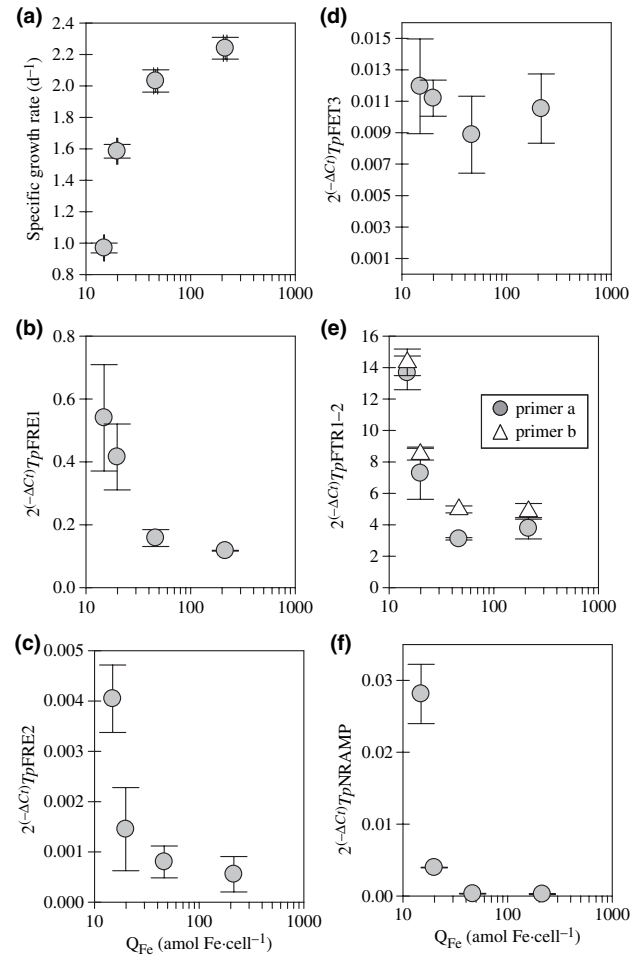


FIG. 9. Growth and relative gene expression (RGE) in *Thalassiosira pseudonana* as a function of cellular Fe quota (Q_{Fe}). (a) Specific growth rate versus Q_{Fe} . (b–f) RGE of various genes versus Q_{Fe} (panel b = *TpFRE1*, c = *TpFRE2*, d = *TpFET3*, e = *TpFTR1-2*, f = *TpNRAMP*). Error bars represent the standard deviations of duplicate RGE determinations (separate QRT-PCR runs) for each treatment. In panel (e), primer pairs a and b refer to those given in Table 1.

Proteins in the NRAMP family have diverse functions despite high similarity, so it is particularly difficult to infer a function of a given NRAMP based on sequence analysis. For example, two rodent NRAMP proteins share 61% homology; yet they have distinct functions—cellular localization and modes of regulation. While NRAMP1 pumps Mn(II) and Fe(II) ions out of macrophages to help kill engulfed pathogens (Vidal et al. 1993, Forbes and Gros 2001), NRAMP2 is involved in transport of dietary Fe(II) (Gunshin et al. 1997). Thus far, this information indicates the likely presence of an NRAMP homologue in *T. pseudonana* but, on its own, does not provide clues as to its function.

Steady-state growth, Fe quota, and gene expression. The growth rate of *P. tricornutum* was Fe limited at 28 and 48 $\mu\text{mol} \cdot \text{L}^{-1}$ Fe' (Fig. 6) in both experiments.

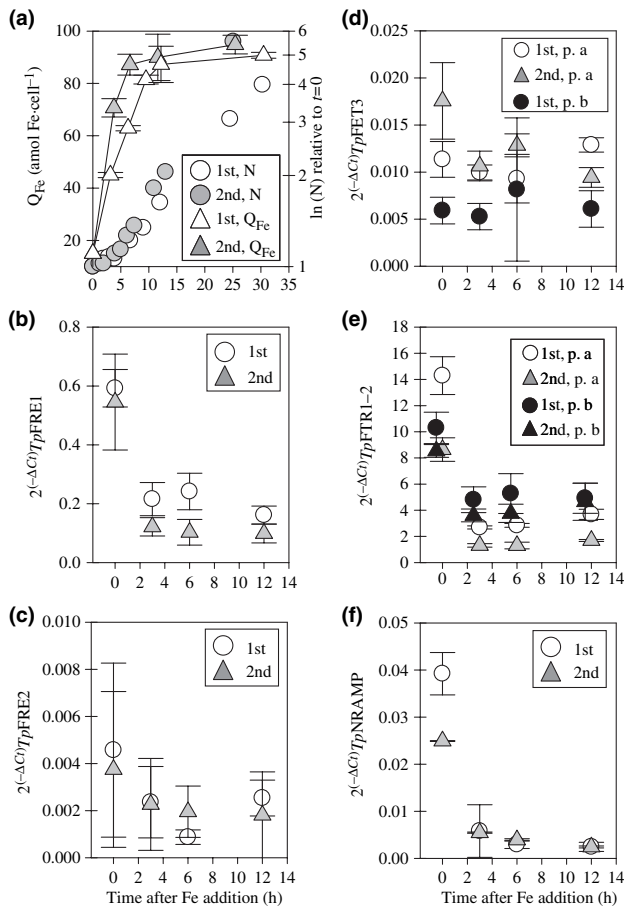


FIG. 10. Cellular Fe accumulation and relative gene expression (RGE) in *Thalassiosira pseudonana* supplied with excessive Fe after growing under low Fe, steady-state conditions. (a) Cellular accumulation of Fe in *T. pseudonana* supplied with excessive Fe (2.44 and $4.12 \text{ nmol} \cdot \text{L}^{-1} \text{ Fe}'$ for experiments 1 and 2) after growing at $170 \text{ pmol} \cdot \text{L}^{-1} \text{ Fe}'$ under steady-state conditions ($t = 0$). Circles indicate changes in cell density (biomass) relative to $t = 0$, triangles indicate Q_{Fe} , and open and closed symbols indicate first and second experiments. Initial cell densities for the first and second experiments were $62,000$ and $171,000 \text{ cells} \cdot \text{mL}^{-1}$, respectively. (b–f) RGE for *T. pseudonana* during Fe-resupply experiments (panel b = *TpFRE1*, c = *TpFRE2*, d = *TpFET3*, e = *TpFTR1-2*, f = *TpNRAMP*). In panels (b), (c), and (f), open circles and grey triangles represent results of the first and second experiments. In panels (d) and (e), p. a and p. b indicate primer pairs A and B, as in Table 1. In (e), data for *TpFTR1-2* primer B were offset by -0.5 h for clarity of presentation.

At Fe' concentrations of $88 \text{ pmol} \cdot \text{L}^{-1}$, growth rate was 89%–96% of maximum. Above this Fe' , cells were growing at maximum growth rate (1.48 – 1.54 d^{-1}) in both experiments. At $88 \text{ pmol} \cdot \text{L}^{-1} \text{ Fe}'$, the cellular iron quota (Q_{Fe}) was 23 – $29 \text{ amol} \cdot \text{cell}^{-1}$. Cultures maintained at or below this cellular quota had steady-state Fe-uptake rates ($V_{ss} = \mu Q_{Fe}$) that were roughly proportional to Fe' , whereas increases in V_{ss} with increasing Fe' appeared and started to plateau above $88 \text{ pmol} \cdot \text{L}^{-1} \text{ Fe}'$ (Fig. 6c). The RGE of both ferric reductases was a direct function of Q_{Fe} and can be generally described by equation (1) from the data

presented in Table 2, where b and a indicate the slope and intercept of the log-log regression of RGE on Q_{Fe} :

$$\text{RGE} = 10^{(b \cdot \log Q_{Fe} + a)} \quad (1)$$

For both *PtFRE1* and *PtFRE2*, this relationship was significant ($P < 0.05$), regardless of which HK gene was used in the analysis (Table 2). Curiously, although growth rates were indistinguishable among cells with quotas of 29, 43, and $46 \text{ amol} \cdot \text{cell}^{-1}$ during the first experiment (Fig. 7a), the RGE for both reductase genes was 9- to 14-fold greater at Q_{Fe} of $29 \text{ amol} \cdot \text{cell}^{-1}$ compared with the higher Fe cells (Fig. 7, b and c). This observation suggests cells growing at $88 \text{ pmol} \cdot \text{L}^{-1} \text{ Fe}'$ were able to maintain maximal growth rate through the induction of a high-affinity uptake system, including ferric reductases. Indeed, in the second experiment at an equal Fe' , Q_{Fe} and growth rate were somewhat lower (Fig. 6, a and b), suggesting that this Fe' provides conditions at the boundary between Fe stress and Fe limitation (we consider Fe stress as the condition at which growth is maximal but there are physiological changes—gene expression, in this case—in response to limiting nutrient concentrations).

The growth rate of *T. pseudonana* was strongly dependent on the Fe concentration in the medium, ranging between 170 and $7200 \text{ pmol} \cdot \text{L}^{-1} \text{ Fe}'$ (Fig. 8a). At Fe' above $1200 \text{ pmol} \cdot \text{L}^{-1}$, cell growth was about 90% of μ_{max} and was therefore only marginally stimulated at higher Fe' . This asymptotic behavior of growth is commonly observed in iron and other nutrient-limitation studies (Sunda and Huntsman 1995). Thus, $\text{Fe}' \sim 1200 \text{ pmol} \cdot \text{L}^{-1}$ appears to be the threshold Fe concentration for *T. pseudonana* growth limitation under our conditions. At this Fe' , a cellular iron quota (Q_{Fe}) of $\sim 50 \text{ amol} \cdot \text{cell}^{-1}$ was obtained in both experiments (Fig. 8b). The steady-state Fe-uptake rate remained proportional to Fe' over the range used in the experiment, except perhaps at the highest Fe' where some saturation of the uptake rate may have been apparent in the second experiment (Fig. 8c). Thus, as often observed, the maximum growth rate was achieved in these cultures at concentrations of iron much below those that saturate the Fe-uptake system of the organism (Morel 1987, Hudson and Morel 1990, Sunda and Huntsman 1995). This finding is due in part to the up-regulation of the uptake system, which compensates for the lower ambient concentration of Fe' .

Thalassiosira pseudonana was much less effective at taking up Fe at low Fe' than *P. tricornutum*. For example, *P. tricornutum* and *T. pseudonana* required 100 ± 9 and $470 \pm 50 \text{ pmol} \cdot \text{L}^{-1} \text{ Fe}'$, respectively, to obtain an uptake rate of $40 \text{ amol} \cdot \text{cell}^{-1} \cdot \text{d}^{-1}$ (Figs. 6c and 8c). This difference is consistent with the ability of *P. tricornutum* to grow at near maximum rates (~ 1.35 – 1.5 d^{-1}) at $88 \text{ pmol} \cdot \text{L}^{-1} \text{ Fe}'$, whereas *T. pseudonana* required $170 \text{ pmol} \cdot \text{L}^{-1} \text{ Fe}'$

TABLE 2. Statistical analyses of effect of cellular Fe quota or Fe resupply on gene expression. (A) Log-log regression of relative gene expression (RGE) on Q_{Fe} within the range of Fe limitation for two reductases in *Phaeodactylum tricornutum*. Data from each biologically replicated experiment were analyzed separately, and three separate housekeeping (HK) genes were used. A reported one-tailed P -value <0.05 indicates the slope of the regression was less than zero, at the 5% significance level, indicating an effect of Q_{Fe} on RGE. (B) Same as (A) except all target transcripts from a *Thalassiosira pseudonana* steady-state experiment were normalized to a single HK gene, actin. (C) Paired comparison of transcript abundances in *T. pseudonana* before Fe addition ($t = 0$ h) and the average abundances after Fe addition ($t = 3, 6, 12$ h).

HK	Target	Slope	(SE)	Intercept	P value
(A) <i>P. tricornutum</i> steady-state experiments					
Actin	<i>PtFRE1</i> , expt. 1	-3.74	0.69	3.54	<0.001
	expt. 2	-2.51	0.27	1.54	<0.0001
TATA	<i>PtFRE1</i> , expt. 1	-3.11	0.56	3.23	<0.001
	expt. 2	-2.43	0.16	2.05	<0.0001
Histone	<i>PtFRE1</i> , expt. 1	-3.44	0.56	3.3	<.0005
	expt. 2	-2.37	0.21	1.68	<0.0001
Actin	<i>PtFRE2</i> , expt. 1	-3.19	0.7	2.92	<0.01
	expt. 2	-2.14	0.35	1.35	<0.001
TATA	<i>PtFRE2</i> , expt. 1	-1.6	0.37	1.42	<0.005
	expt. 2	-2.14	0.38	1.9	<0.005
Histone	<i>PtFRE2</i> , expt. 1	-2.22	0.44	1.88	<0.005
	expt. 2	-2.16	0.38	1.64	<0.005
(B) <i>T. pseudonana</i> steady-state experiments					
Actin	<i>TpFRE1</i>	-1.08	0.18	1	<0.005
	<i>TpFRE2</i>	-1.27	0.45	-1.04	<0.05
	<i>TpFTR1-a</i>	-1.23	0.16	2.53	<0.001
	<i>TpFTR1-b</i>	-0.86	0.12	2.12	<0.001
	<i>TpFET3-b</i>	-0.27	0.17	-1.6	0.0885
	<i>TpNRAMP</i>	-3.72	0.39	2.65	<0.001
HK	Target	P value	n		
(C) <i>T. pseudonana</i> Fe-resupply experiments					
Actin	<i>TpFRE1</i>	<0.005	4		
	<i>TpFRE2</i>	<0.05	6		
	<i>TpFET3-a</i>	0.375	3		
	<i>TpFET3-b</i>	0.108	4		
	<i>TpFTR1-a</i>	<0.005	4		
	<i>TpFTR1-b</i>	<0.0005	4		
	<i>TpNRAMP</i>	<0.005	4		

to grow at $\sim 1.0 \text{ d}^{-1}$. A comparison of uptake rate versus Fe' in regions of common Fe' (Figs. 6a and 8a) indicates a ~ 4 - to 5-fold increase in uptake rate for *P. tricornutum* compared with *T. pseudonana*. Although we did not measure *P. tricornutum* cell surface area, these cells are similarly sized, and this difference in uptake rate is too large to be attributed to any differences in cell surface area.

The RGE for *TpFRE1* and *TpFRE2* was significantly greater at low Q_{Fe} compared with high Q_{Fe} (Fig. 9, a and b; Table 2B). For *TpFRE1*, this up-regulation was evident even at $Q_{Fe90\%}$ ($50 \text{ amol} \cdot \text{cell}^{-1}$; Fig. 9a). *TpFRE1* seems to be a much more abundant transcript than *TpFRE2*, suggesting that the corresponding reductase (*TpFRE1p*) may play a more significant role under low Fe. In addition, *TpFRE1* transcripts are relatively abundant even at maximum, Fe-replete growth rates (Fig. 9, a and b) and are therefore inducible at low Fe and constitutively expressed at high Fe.

Permease expression levels are clearly controlled by Q_{Fe} , as indicated by two separate primer pairs for *TpFTR1-2* (Fig. 9e; Table 2B). These genes are induced by low Q_{Fe} (RGE ~ 8 –10) and also have a

high level of constitutive expression (RGE ~ 3 –4) at high Q_{Fe} . The expression profile of the ferroxidase (*TpFET3*) gene under steady-state conditions revealed a slight negative trend with Q_{Fe} , but this trend was not significant at the 5% level ($P = 0.0885$; Fig. 9d; Table 2B). It is well recognized that cellular protein levels in eukaryotes are often controlled by a combination of transcriptional and posttranscriptional processes. Because of this fact, differences in protein levels may not always be represented by differences in gene transcripts quantified under steady-state conditions. Therefore, we also evaluated gene expression in *T. pseudonana* under conditions of rapidly changing Fe availability (below).

TpNRAMP was regulated by cellular Fe status to a much greater extent in steady-state experiments than some of the genes putatively involved in the reductive/oxidative pathway of Fe uptake (Fig. 9f). Although *TpNRAMP* transcripts were much less abundant than those for *TpFRE1* and *TpFTR1-2*, *TpNRAMP* transcripts showed the most dramatic down-regulation of all the genes considered [comparing the slopes obtained by eq. (1); Table 2B].

This trend is because *Tp*NRAMP transcripts were virtually undetectable at $Q_{Fe90\%}$, whereas *Tp*FRE1 and *Tp*FTR1-2 showed significant levels of constitutive expression under our conditions.

Transient gene expression. Fe availability was varied over short-time scales in cultures of *T. pseudonana* to elucidate better the regulatory role of cellular Fe on gene regulation. In both Fe-resupply experiments, Q_{Fe} increased dramatically between time zero and ~3 h (Fig. 10a); at 3 h the Q_{Fe} approached or exceeded $Q_{Fe90\%}$ (from Fig. 8, a and b) and continued increasing until about 10 h (Fig. 10a). Q_{Fe} did not increase throughout the remainder of the experiment, consistent with a down-regulation of the Fe-uptake machinery. Growth rates also responded to the Fe additions, but only after an initial lag phase of about 4–5 h.

Between the beginning of the experiments and ~3 h after Fe addition, the RGE of most transcripts under consideration dropped to levels that were more or less maintained throughout the rest of the experiment. Paired comparisons of time zero versus time 3–12 h RGE data revealed significantly lower transcript abundances for *Tp*FRE1, *Tp*FRE2, *Tp*FTR1-2, and *Tp*NRAMP after Fe addition ($P < 0.05$ – 0.0005 ; Table 2C; Fig. 10, b, c, e, and f). However, we observed no significant decrease in transcript abundance of *Tp*FET3 between time zero and 3–12 h (Fig. 10d; Table 2C; one-tailed P -value = 0.375, $P = 0.108$), using two separate primers (Table 1). This finding is consistent with our observations in the *T. pseudonana* steady-state experiment (Fig. 9d).

*Tp*NRAMP transcripts showed the most dramatic down-regulation upon Fe addition: *Tp*NRAMP transcript abundance after 3 h was only ~4% of the initial value. This 25-fold down-regulation of NRAMP did not change throughout the remainder of the experiment.

There was an excellent agreement between the mean RGE levels at time zero (where $Fe' = 170 \mu\text{mol} \cdot \text{L}^{-1}$) in these experiments and the RGE levels at the same Fe' in the steady-state experiments (Fig. 9, b–f), attesting to the overall reproducibility of our results. We did, however, experience variability in our analysis of transcript abundances from one QRT–PCR run to another (this was most evident in our analysis of *Tp*FRE2 during the Fe-resupply experiments). However, the paired comparisons for the Fe-resupply experiments are insensitive to the systematic variability from one QRT–PCR run to another, and the abundance of *Tp*FRE2 transcripts (and all other transcripts of interest except *Tp*FET3) decreased significantly after Fe resupply.

Inhibitors of metal uptake. The high-affinity Fe-uptake system of yeast is fairly specific for Fe, as the only other metal known to react with cell-surface reductases and oxidases is Cu (Fig. 1). In contrast, Fe uptake mediated by NRAMP and other divalent metal transporters can be inhibited by other metals

TABLE 3. Summary of Fe-uptake experiments with *Thalassiosira pseudonana* and *Phaeodactylum tricornutum* (for brevity, *Thaps* and *Phatr*, respectively).

Experiment/treatment	Fe uptake
(A) $Fe' = 408$	
<i>Thaps</i> control	6.23×10^{-19} (0.73)
<i>Thaps</i> + 20 BCDS	5.11×10^{-19} (0.59)
<i>Thaps</i> + 5 Cu	-3.45×10^{-21} (3.6)*
<i>Thaps</i> + 5 Cu, 20 BCDS	5.25×10^{-20} (3.1)*
(B) $Fe' = 408$	
<i>Thaps</i> control	3.44×10^{-19} (0.26)
<i>Thaps</i> + 10 BCDS	3.31×10^{-19} (0.66)
<i>Thaps</i> + 0.5 Cu	1.06×10^{-19} (0.58)*
<i>Thaps</i> + 0.5 Cu, 10 BCDS	4.58×10^{-19} (0.15)†
(C) $Fe' = 408$	
<i>Thaps</i> control	5.89×10^{-19} (0.55)
<i>Thaps</i> + 2.5 Cd	5.83×10^{-19} (0.23)
<i>Thaps</i> + 2.5 Mn	6.74×10^{-19} (0.10)
<i>Thaps</i> + 2.5 Zn	5.41×10^{-19} (0.46)
(D) $Fe' = 68$	
<i>Phatr</i> control	1.03×10^{-18} (0.06)
<i>Phatr</i> + 2.5 Cd	8.05×10^{-19} (1.55)
<i>Phatr</i> + 2.5 Mn	1.03×10^{-18} (0.05)
(E) $Fe' = 28$	
<i>Phatr</i> control	2.48×10^{-18} (0.26)
<i>Phatr</i> + 10 BCDS	1.85×10^{-18} (0.35)
<i>Phatr</i> + 0.5 Cu	4.65×10^{-19} (1.62)*
<i>Phatr</i> + 0.5 Cu, 10 BCDS	1.80×10^{-18} (0.46)†
(F) $Fe' = 28$	
<i>Phatr</i> control	3.48×10^{-18} (1.0)
<i>Phatr</i> + 2.5 Cd	3.32×10^{-18} (0.60)
<i>Phatr</i> + 10 Cd	3.44×10^{-18} (1.52)
<i>Phatr</i> + 0.5 Zn	4.33×10^{-18} (0.29)
<i>Phatr</i> + 1.5 Zn	3.32×10^{-18} (0.52)
(G) $Fe' = 28$	
<i>Phatr</i> control	3.45×10^{-18} (0.15)
<i>Phatr</i> + 2.5 Zn	3.30×10^{-18} (0.24)
<i>Phatr</i> + 10 Cd	3.50×10^{-18} (0.38)

Fe-uptake rates were determined from time series measurements (reported as $\text{mol Fe} \cdot \text{cell}^{-1} \cdot \text{h}^{-1}$) conducted in chelated synthetic ocean water with $500 \mu\text{mol} \cdot \text{L}^{-1}$ added $^{59}\text{FeCl}_3$. Brackets represent the standard error of each slope (expressed in the same power of 10 as the rate). Cell densities (expressed as $1000 \text{ cells} \cdot \text{mL}^{-1}$) for experiments A–G were 10, 10, 20, 1.5, 10, 21.7, and 10, respectively. The Fe' concentration (in $\mu\text{mol} \cdot \text{L}^{-1}$) of each source culture is indicated beneath the experiment number. All metal and ligand concentrations are given in $\mu\text{mol} \cdot \text{L}^{-1}$. Asterisks (*) indicate a significant difference from control rate, and cross-hatching (†) indicates a significant recovery of uptake rate from Cu-only treatments. BCDS, bathocuproine disulfonic acid.

at varying degrees. We thus tested whether these metals would inhibit uptake of $Fe(\text{III})'$ in *T. pseudonana* or *P. tricornutum*. A concentration of $2.5 \mu\text{mol} \cdot \text{L}^{-1}$ Mn(II), Zn(II), or Cd(II) did not inhibit uptake in either species (Table 3; experiments C, D, F, G), as might have been expected if $Fe(\text{II})$ transport involved a divalent metal transporter that is as nonspecific as observed in $Fe(\text{II})$ transporters from other systems. Addition of $5 \mu\text{mol} \cdot \text{L}^{-1}$ Cu(II) was tested in *T. pseudonana*, and this completely abolished Fe uptake in this diatom (experiment A). In subsequent experiments, $0.5 \mu\text{mol} \cdot \text{L}^{-1}$ Cu(II) additions inhibited Fe uptake by 70%–80% in both species (experiments B

and E, respectively). BCDS in the presence of $0.5 \mu\text{mol} \cdot \text{L}^{-1}$ Cu restored Fe-uptake rates in both species (experiments B and E). Thus, the effect of Cu on Fe uptake appears to be caused by Cu(I) [presumably produced from Cu(II) by the reductases or superoxide in the medium; Jones et al. 1987, Kustka et al. 2005], perhaps by interfering with an oxidase involved in Fe transport. At the concentrations that were used, Cu had no effect on ^{14}C -fixation rates in either species (data not shown), making it improbable that the effect of Cu resulted from a general metabolic inhibition.

DISCUSSION

The responses that we observed in the growth rates, in Fe uptake, and in the expression of genes putatively involved in the Fe acquisition in *T. pseudonana* and *P. tricornutum* appear consistent with each other and provide insight into the mechanisms of Fe uptake in diatoms.

The relative expression of the reductase genes in both diatoms, and the permease and NRAMP genes in *T. pseudonana*, is directly related to the cellular Fe quotas in the steady-state experiments (Figs. 7 and 9; Table 2, A and B). The transcriptional responses upon increasing Fe availability are relatively rapid and also consistent with the rapid increase in cellular Fe quota (Table 2C; Fig. 10). Down-regulation of gene expression after Fe resupply was complete after 3 h, while the cellular Fe quota had approached or exceeded the quota necessary for μ_{max} under steady-state growth conditions (comparing Figs. 10a and 8b). The intracellular Fe that may be sensed by iron-responsive transcriptional factors may be greater during an Fe-resupply experiment than under replete steady-state conditions when the bulk of the Fe is sequestered in active metabolic pathways. Although the cells had sufficient Fe for maximal growth at 3 h, the increase in growth rate was not apparent for another few hours. This decoupling between cellular Fe quota and growth rate is expected, as the diatom presumably requires time to rebuild its biochemical machinery. In Fe-resupply experiments with the green alga *Dunaliella tertiolecta* Butcher, Greene et al. (1992) observed that at least 3–5 h were required for the de novo synthesis of cytochrome b_6/f complex (a major fraction of the cellular Fe quota), and longer timescales (10–15 h) were required for D1 protein synthesis in *D. tertiolecta* or *P. tricornutum*. It is also notable that a rapid rate of Fe uptake was maintained in the Fe-resupply experiment for several hours after down-regulation of the transcription of the relevant genes. This finding reflects the longevity of the proteins themselves and possibly a regulation of their activities that is distinct from that of gene transcription.

Anderson and Morel (1982) first noted that the strong Fe(II)-complexing ligand BCDS inhibited Fe

uptake in *T. weissflogii* in an EDTA-buffered system. Since then, there has been increasing evidence that inducible reductive processes are involved in Fe acquisition from a variety of Fe species in marine diatoms (Soria-Dengg and Horstmann 1995, Maldonado and Price 1999, 2001, Shaked et al. 2005) and other photosynthetic protists (Allnutt and Bonner 1987, Weger and Espie 2000). Our analysis of transcript abundance demonstrates the regulation of reductase gene expression in two diatoms in response to Fe availability. Despite some differences between the putative reductases identified in *T. pseudonana* and *P. tricornutum* and those of model organisms (Fig. 2), there is little doubt that cell surface reductases are involved as a first step in Fe acquisition by diatoms.

The transport of Fe(II) produced by the reductases in diatoms may be accomplished by a system akin to the ferroxidase/permease in various fungi and *Chlamydomonas* (Fig. 1) as has been previously suggested (Maldonado and Price 2001, Shaked et al. 2005, Maldonado et al. 2006). However, this does not preclude the possibility that divalent metal ion transporters may also participate in Fe(II) transport in some species, depending on the ambient physical and chemical conditions. The ferroxidase/permease transporter may also be missing from some phytoplankton species altogether. Here we discuss the lines of evidence in support of and against the existence of a ferroxidase/permease transport system in the two species we studied.

In *T. pseudonana*, the weight of evidence supports a ferroxidase/permease pathway for Fe(II) transport. Putative genes for permeases and a ferroxidase are present in the genome. Peers et al. (2005) determined that *T. weissflogii* and *T. oceanica* (congeners of *T. pseudonana*) have lower steady-state Fe-uptake rates at low concentrations of Cu, which is required for synthesis of the ferroxidase. More recently, Maldonado et al. (2006, table 4) also observed an effect of Cu availability on uptake of ferrioxamine-bound Fe in both *T. pseudonana* and *T. oceanica*. Further, our metal inhibition data are consistent with Fe(II) transport via a ferroxidase/permease. The only experimental result that does not support a ferroxidase/permease pathway in *T. pseudonana* is the lack of regulation of *TpFET3* in our study. But our results differ from those of Maldonado et al. (2006), who found a 60-fold increase in *TpFRE3* transcripts in cells grown at pFe 20.5 compared with pFe 19 (corresponding to 40 and 1300 $\text{pmol} \cdot \text{L}^{-1}$ Fe', respectively; Sunda et al. 2005). This difference between our result and that of Maldonado et al. may be due to a difference in the extent of Fe limitation, as our most Fe-limited *T. pseudonana* treatment was grown at 170 $\text{pmol} \cdot \text{L}^{-1}$ Fe'.

In *P. tricornutum*, while there is strong evidence for the involvement of a cell-surface reductase under low Fe, there is very little experimental support for a ferroxidase/permease transport system.

The only evidence consistent with the involvement of a ferroxidase-like enzyme is the inhibition of Fe uptake by Cu(II) that is relieved by scavenging Cu(I), as also observed in *T. pseudonana*. However, this evidence is too indirect to outweigh the simple fact that we did not identify homologues for a ferroxidase or a permease in the genome of *P. tricornutum*. It is, of course, possible that proteins analogous to ferroxidase and permease involved in Fe(II) transport (Fig. 1) could not be identified in *P. tricornutum* because of insufficient similarity with the corresponding proteins in model organisms. But this possibility seems unlikely in view of the fairly well-conserved motifs in these proteins, particularly in multi-copper oxidases (Fig. 3; Murphy et al. 1997). So the Fe-uptake systems of *P. tricornutum* and *T. pseudonana* appear to be fundamentally different from each other. This difference is supported by the seemingly more efficient uptake of Fe' observed in *P. tricornutum*.

The strong response of NRAMP gene expression in *T. pseudonana* brings up the question of the function of NRAMP in this organism. We did not observe any inhibition of Fe uptake at micromolar concentrations of other divalent metals, suggesting that NRAMP may not have been involved in cell-surface Fe(II) transport. It is possible that NRAMP might be up-regulated for the opportunity of cell-surface uptake, but it may be ineffective at taking up Fe(II) under our assay conditions (0.5 nM Fe(III)' in the dark at pH \geq 8, 23°C), where Fe(II) in the bulk medium is scarce and should oxidize to Fe(III) before reacting with cell-surface ligands (see Shaked et al. 2005 and Kustka et al. 2005 for a more thorough discussion). Up-regulation of multiple Fe-uptake systems would be advantageous in an environment with episodic Fe supply, especially in cold waters where Fe(II) oxidation rates are slow. A second possibility is that NRAMP may play a role in Fe metabolism entirely different from cell-surface uptake. Some NRAMP homologues in *A. thaliana* and in *S. cerevisiae* may be involved in mobilizing iron out of intracellular vacuoles (Portnoy et al. 2000, Thomine et al. 2003) and are up-regulated under low Fe. Such a role would be consistent with the lack of inhibition of Fe uptake by other divalent metals.

This investigation into gene expression in *T. pseudonana* and *P. tricornutum* as a function of Fe nutrition identifies some of the proteins that are probably responsible for Fe uptake and points out differences that may exist between the Fe-uptake machinery of different classes of diatoms. According to field data, pennate diatoms appear to be more competitive in low-Fe environments. For example, Tsuda et al. (2003) showed that centric diatoms bloomed in the northwestern Pacific Ocean during the SEEDS Fe fertilization experiment, yet these centric diatoms subsided and pennates again became dominant as the dissolved Fe returned to

preaddition concentrations. These authors point out that pennates are the successful diatoms in regions of chronically low Fe, such as the Southern Ocean and subarctic Pacific. Our data suggest that perhaps there are mechanistic differences in the Fe-uptake systems of pennate and centric diatoms; these differences might in turn be responsible for niche differentiation in oceanic systems with varied Fe supply. A thorough understanding of the factors that control the relative success of phytoplankton species in Fe-limited environments and their differential responses to Fe supply requires an elucidation of the mechanisms by which various species acquire Fe.

We thank Chris Bowler for providing access to the *Phaeodactylum tricornutum* genome and EST data base. The authors thank Bess Ward for use of the Q-PCR machine. This work was supported by funding from the Center for Environmental Bioinorganic Chemistry (NSF CHE# 0221978).

- Agranoff, D., Collins, L., Kehres, D., Harrison, T., Maguire, M. & Krishna, S. 2005. The Nramp orthologue of *Cryptococcus neoformans* is a pH-dependent transporter of manganese, iron, cobalt and nickel. *Biochem. J.* 385:225–32.
- Allnut, F. C. T. & Bonner, W. D. 1987. Evaluation of reductive release as a mechanism for iron uptake from ferrioxamine B by *Chlorella vulgaris*. *Plant Physiol.* 85:751–6.
- Anderson, M. A. & Morel, F. M. M. 1982. The influence of aqueous iron chemistry on the uptake of iron by the coastal *Thalassiosira weissflogii*. *Limnol. Oceanogr.* 27:789–813.
- Armbrust, E. V., Berges, J. A., Bowler, C., Green, B. R., Martinez, D., Putnam, N. H., Zhou, S., et al. 2004. The genome of the diatom *Thalassiosira pseudonana*: ecology, evolution, and metabolism. *Science* 306:79–86.
- Beszteri, B., Acs, E., Makk, J., Kovacs, G., Marialigeti, K. & Kiss, K. T. 2001. Phylogeny of six naviculoid diatoms based on 18S rDNA sequences. *Int. J. Syst. Evol. Microbiol.* 51:1581–6.
- Bustin, S. A. 2002. Quantification of mRNA using real-time reverse transcription PCR (RT-PCR): trends and problems. *J. Mol. Endocrinol.* 29:23–39.
- Cellier, M., Prive, G., Belouchi, A., Kwan, T., Rodrigues, V., Chia, W. & Gros, P. 1995. Nramp defines a family of membrane-proteins. *Proc. Natl Acad. Sci. U. S. A.* 92:10089–93.
- Cohen, C. K., Garvin, D. F. & Kochian, L. V. 2004. Kinetic properties of a micronutrient transporter from *Pisum sativum* indicate a primary function in Fe uptake from the soil. *Planta* 218:784–92.
- Eckhard, U., Marques, A. M. & Buckhout, T. J. 2001. Two iron-regulated cation transporters from tomato complement metal uptake-deficient yeast mutants. *Plant Mol. Biol.* 45:437–48.
- Eide, D. J. 1998. The molecular biology of metal ion transport in *Saccharomyces cerevisiae*. *Annu. Rev. Nutr.* 18:441–69.
- Eide, D., Broderius, M., Fett, J. & Guerinot, M. L. 1996. A novel iron-regulated metal transporter from plants identified by functional expression in yeast. *Proc. Natl Acad. Sci. U. S. A.* 93:5624–8.
- Fang, H. M. & Wang, F. 2002. Characterization of iron-binding motifs in *Candida albicans* high-affinity iron permease CaFtr1p by site-directed mutagenesis. *Biochem. J.* 368:641–7.
- Finegold, A. A., Shatwell, K. P., Segal, A. W., Klausner, R. D. & Dancis, A. 1996. Intramembrane bis-heme motif for transmembrane electron transport conserved in a yeast iron reductase and the human NADPH oxidase. *J. Biol. Chem.* 271:31021–4.
- Forbes, J. R. & Gros, P. 2001. Divalent-metal transport by NRAMP proteins at the interface of host-pathogen interactions. *Trends Microbiol.* 9:397–403.
- Fu, Y., Lee, H., Collins, M., Tsai, H.-F., Spellberg, B., Edwards, J. E., Jr., Kwon-Chung, K. J. & Ibrahim, A. S. 2004. Cloning and

- functional characterization of the *Rhizopus oryzae* high affinity iron permease (rFTR1) gene. *FEMS Microbiol. Lett.* 235:169–76.
- Greene, R. M., Geider, R. J., Kobler, Z. & Falkowski, P. G. 1992. Changes in light harvesting and photochemical energy conversion processes in eukaryotic marine algae. *Plant Physiol.* 100:565–75.
- Gunshin, H., MacKenzie Berger, U. V., Gunshin, Y., Romero, M. F., Boron, W. F., Nussberger, S., Gollan, J. L. & Hediger, M. A. 1997. Cloning and characterization of a mammalian proton-coupled metal-ion transporter. *Nature* 388:482–8.
- Herbik, A., Bolling, C. & Buckhout, T. J. 2002. The involvement of a multicopper oxidase in iron uptake by the green algae *Chlamydomonas reinhardtii*. *Plant Physiol.* 130:2039–48.
- Hudson, R. J. M. & Morel, F. M. M. 1989. Distinguishing between extra- and intracellular iron in marine phytoplankton. *Limnol. Oceanogr.* 34:1113–20.
- Hudson, R. J. M. & Morel, F. M. M. 1990. Iron transport in marine phytoplankton: kinetics of cellular and medium coordination reactions. *Limnol. Oceanogr.* 35:1002–20.
- Ikedo-Saito, M., Hori, H., Andersson, L. A., Prince, R. C., Pickering, I. J., George, G. N., Sanders, C. R., III, Lutz, R. S., McKelvey, E. J. & Mattera, R. 1992. Coordination structure of the ferric heme iron in engineered distal histidine myoglobin mutants. *J. Biol. Chem.* 267:22843–52.
- Jones, G. J., Palenik, B. & Morel, F. M. M. 1987. Trace metal reduction by phytoplankton: the role of plasmalemma redox enzymes. *J. Phycol.* 23:237–44.
- Kosman, D. J. 2003. Molecular mechanisms of iron uptake in fungi. *Mol. Microbiol.* 47:1185–97.
- Krogh, A., Larsson, B., von Heijne, G. & Sonhammer, E. L. L. 2001. Predicting transmembrane protein topology with a hidden Markov model: application to complete genomes. *J. Mol. Biol.* 305:567–80.
- Kustka, A. B., Shaked, Y., Milligan, A. J., King, D. W. & Morel, F. M. M. 2005. Extracellular superoxide production by marine diatoms: contrasting effects on iron redox chemistry and bioavailability. *Limnol. Oceanogr.* 50:1172–80.
- La Fontaine, S., Quinn, J. M., Nakamoto, S. S., Page, M. D., Gohre, V., Mosely, J. L., Kropat, J. & Merchant, S. 2002. Copper-dependent iron assimilation pathway in the model photosynthetic eukaryote *Chlamydomonas reinhardtii*. *Eukaryot. Cell* 1:736–57.
- Maldonado, M. T., Allen, A. E., Chong, J. S., Lin, K., Dan, L. M., Karpenko, N. & Harris, S.L. 2006. Copper dependent iron uptake in coastal and oceanic diatoms. *Limnol. Oceanogr.* 41:1729–43.
- Maldonado, M. T. & Price, N. M. 1999. Utilization of iron bound to strong organic ligands by plankton communities in the subarctic Pacific Ocean. *Deep-Sea Res. Part II Top. Stud. Oceanogr.* 46:2447–73.
- Maldonado, M. T. & Price, N. M. 2001. Reduction and transport of organically bound iron by *Thalassiosira oceanica* (Bacillariophyceae). *J. Phycol.* 37:298–309.
- Martin, J. H. & Fitzwater, S. E. 1988. Iron deficiency limits phytoplankton growth in the north-east Pacific subarctic. *Nature* 331:341–3.
- Martin, J. H., Coale, K. H., Johnson, K. S., Fitzwater, S. E., Gordon, R. M., Tanner, S. J., Hunter, C. N., et al. 1994. Testing the iron hypothesis in ecosystems of the equatorial Pacific Ocean. *Nature* 371:123–9.
- Moore, J. K., Doney, S. C., Glover, D. M. & Fung, I. Y. 2002. Iron cycling and nutrient-limitation patterns in surface waters of the World Ocean. *Deep-Sea Res. Part II Top. Stud. Oceanogr.* 49:463–507.
- Morel, F. M. M. 1987. Kinetics of nutrient uptake and growth in phytoplankton. *J. Phycol.* 23:137–50.
- Murphy, M. E. P., Lindley, P. F. & Adman, E. T. 1997. Structural comparison of cupredoxin domains: domain recycling to construct proteins with novel functions. *Protein Sci.* 6:761–70.
- Nelson, D. M., Treguer, P., Brzezinski, M. A., Leynaert, A. & Queguiner, B. 1995. Production and dissolution of biogenic silica in the ocean: revised global estimates, comparison with regional data and relationship to biogenic sedimentation. *Glob. Biogeochem. Cycles* 9:359–72.
- Peers, G., Quesnel, S. A. & Price, N. M. 2005. Copper requirements for iron acquisition and growth of coastal and oceanic diatoms. *Limnol. Oceanogr.* 50:1149–58.
- Pfaffl, M. W. 2001. A new mathematical model for relative quantification in real-time RT-PCR. *Nucleic Acids Res.* 29:e45.
- Portnoy, M. E., Liu, X. F. & Culotta, V. C. 2000. *Saccharomyces cerevisiae* expresses three functionally distinct homologues of the Nramp family of metal transporters. *Mol. Cell. Biol.* 20:7893–902.
- Rosakis, A. & Koster, W. 2005. Divalent metal transport in the green microalga *Chlamydomonas reinhardtii* is mediated by a protein similar to prokaryotic Nramp homologues. *Biomaterials* 18:107–20.
- Severance, S., Chakraborty, S. & Kosman, D. J. 2004. The Ftr1p iron permease in the yeast plasma membrane: orientation, topology and structure-function relationships. *Biochem. J.* 380:487–96.
- Shaked, Y., Kustka, A. B. & Morel, F. M. M. 2005. A general kinetic model for iron acquisition by eukaryotic phytoplankton. *Limnol. Oceanogr.* 50:872–82.
- Shatwell, K. P., Dancis, A., Cross, A. R., Klausner, R. D. & Segal, A. W. 1996. The FRE1 ferric reductase of *Saccharomyces cerevisiae* is a cytochrome *b* similar to that of NADPH oxidase. *J. Biol. Chem.* 271:14240–4.
- Shi, X. L., Stoj, C., Romeo, A., Kosman, D. J. & Zhu, Z. W. 2003. Fre1p Cu²⁺ reduction and Fet3p Cu¹⁺ oxidation modulate copper toxicity in *Saccharomyces cerevisiae*. *J. Biol. Chem.* 278:50309–15.
- Sokal, R. R. & Rohlf, F. J. 1995. *Biometry*. 3rd ed. W. H. Freeman and Co., New York, 887pp.
- Soria-Dengg, S. & Horstmann, U. 1995. Ferrioxamine B and E as iron sources for the marine diatom *Phaeodactylum tricorutum*. *Mar. Ecol. Prog. Ser.* 125:269–77.
- Stoj, C. & Kosman, D. J. 2003. Cuprous oxidase activity of yeast Fet3p and human ceruloplasmin: implication for function. *FEBS Lett.* 554:422–6.
- Sunda, W. G. & Huntsman, S. A. 1995. Iron uptake and growth limitation in oceanic and coastal phytoplankton. *Mar. Chem.* 50:189–206.
- Sunda, W., Price, N. M. & Morel, F. M. M. 2005. Trace metal ion buffers and their use in culture studies. In Anderson, R. [Ed.] *Algal Culturing Techniques*. Academic Press, Burlington, MA, pp. 35–63.
- Tanaka, M., Ishimori, K., Mukai, M., Kitagawa, T. & Morishima, I. 1997. Catalytic activities and structural properties of horseradish peroxidase distal His42>Glu or Gln mutant. *Biochemistry* 36:9889–98.
- Taylor, A. B., Stoj, C. S., Ziegler, L., Kosman, D. J., Hart, P. J. 2005. The copper-iron connection in biology: structure of the metallo-oxidase Fet3p. *Proc. Natl. Acad. Sci. U. S. A.* 102:15459–64.
- Thomine, S., Lelievre, F., Debarbieux, E., Schroeder, J. I. & Barbier-Brygoo, H. 2003. AtNRAMP3, a multispecific vacuolar metal transporter involved in plant responses to iron deficiency. *Plant J.* 34:685–95.
- Thomine, S., Wang, R. C., Ward, J. M., Crawford, N. M. & Schroeder, J. I. 2000. Cadmium and iron transport by members of a plant metal transporter family in *Arabidopsis* with homology to Nramp genes. *Proc. Natl. Acad. Sci. U. S. A.* 97:4991–6.
- Tsuda, A., Takeda, S., Saito, H., Nishioka, J., Nojiri, Y., Kudo, I., Kiyosawa, H., et al. 2003. A mesoscale iron enrichment in the western subarctic Pacific induces a large centric diatom bloom. *science* 300:958–61.
- Vidal, S. M., Malo, D., Vogan, K., Skamene, E. & Gros, P. 1993. Natural resistance to infection with intracellular parasites: isolation of a candidate for Bcg. *Cell* 73:469–85.
- Weger, H. G. & Espie, G. S. 2000. Ferric reduction by iron-limited *Chlamydomonas* cells interacts with both photosynthesis and respiration. *Planta* 210:775–81.